Super-resolution microscopy of mitochondrial mRNAs

Stefan Stoldt[1,2,3,*], Frederike Maass[1,2,3,*], Michael Weber[4], Sven Dennerlein[5], Peter Ilgen[1,2,6], Jutta Gärtner[3,6,7], Aysenur Canfes[1,2], Sarah V. Schweighofer[1,6], Daniel C. Jans[1,2], Peter Rehling[3,5,6,8], Stefan Jakobs[1,2,3,6,#]

[1]Department of NanoBiophotonics, Max Planck Institute for Multidisciplinary Sciences, RG Mitochondrial Structure and Dynamics, Göttingen, Germany

[2]Clinic of Neurology, University Medical Center Göttingen, Göttingen, Germany

[3]Cluster of Excellence "Multiscale Bioimaging: from Molecular Machines to Networks of Excitable Cells" (MBExC), University of Göttingen, Göttingen, Germany

[4]Department of NanoBiophotonics, Max Planck Institute for Multidisciplinary Sciences, Göttingen, Germany

[5]Department of Cellular Biochemistry, University Medical Center Göttingen, Göttingen, Germany

[6]Fraunhofer Institute for Translational Medicine and Pharmacology, Translational Neuroinflammation and Automated Microscopy, Göttingen, Germany

[7]Department of Pediatrics and Adolescent Medicine, University Medical Center Göttingen, Göttingen, Germany

[8]Max Planck Institute for Multidisciplinary Sciences, Göttingen, Germany

*These authors contributed equally

[#]Correspondence to SJ (sjakobs@gwdg.de)

Abstract

Mitochondria contain their own DNA (mtDNA) and a dedicated gene expression machinery. As the mitochondrial dimensions are close to the diffraction limit of classical light microscopy, the spatial distribution of mitochondrial proteins and in particular of mitochondrial mRNAs remains underexplored. Here, we establish single-molecule fluorescence in situ hybridization (smFISH) combined with STED and MINFLUX super-resolution microscopy (nanoscopy) to visualize individual mitochondrial mRNA molecules and associated proteins. STED nanoscopy revealed the spatial relationships between distinct mRNA species and proteins such as the RNA granule marker GRSF1, demonstrating adaptive changes in mRNA distribution and quantity in challenged mammalian cells and patient-derived cell lines. Notably, STED-smFISH showed the release of mRNAs during apoptosis, while MINFLUX revealed the folding of the mRNAs into variable shapes, as well as their spatial proximity to mitochondrial ribosomes. These protocols are transferable to various cell types and open new avenues for understanding mitochondrial gene regulation in health and disease.

Introduction

Mitochondria are unique eukaryotic organelles, as they contain their own DNA (mtDNA). The mtDNA is a gene-dense circular DNA molecule of about 16.6 kilobases. A single mtDNA is compacted by proteins into a structure termed nucleoid, of which several hundred up to a few thousand exist in a cell[1-4].

The mitochondrial gene expression machinery that mediates the synthesis of only 13 proteins has a remarkable complexity and differs substantially both from the nuclear as well as from the bacterial machineries [5,6]. The mitochondrial DNA-directed RNA polymerase (POLRMT) initiates transcription on the light- and the heavy-strand, producing near genome-length polycistronic transcripts that encompass all of the coding information of the respective strand[5,7]. Whereas 12 mRNAs, encoding for subunits of the oxidative phosphorylation system (OXPHOS), two rRNAs, and 14 tRNAs are transcribed from the heavy strand, only one mRNA (*MT-ND6*), eight tRNAs, and several non-coding RNAs are transcribed from the light strand[8,9].The polycistronic transcripts produced are processed within distinct foci, referred to as mitochondrial granules, to generate individual mRNAs, tRNAs, and rRNAs [10-12]. Biochemical analysis demonstrated low steady-state levels of the unprocessed transcripts, suggesting that processing of the transcripts occurs co-transcriptionally[13].

However, fundamental questions regarding the spatial distribution of the gene expression machinery in human mitochondria remain underexplored. In budding yeast, it has been shown that specific transcripts are preferentially translated at distinct sites within the mitochondrial inner membrane[14]. Yet, the sub-mitochondrial localizations and amounts of mitochondrial transcripts in individual mitochondria are unknown. Also, the spatial relation of specific mRNAs to nucleoids or to the RNA granules are not known and the level of mRNA compaction within mitochondria has not been investigated. Although high-resolution profiling of mitochondrial translation and cryoelectron tomography suggested the existence of mitochondrial polysomes in human mitochondria[15,16], the existence of mitochondrial polysomes is still not conclusively proven. Arguably, to answer such questions, imaging is required. Although various fluorescent in situ hybridization (FISH) methods have been established for the study of cytoplasmic mRNAs, these approaches have been used very little to study mitochondrial transcripts[10,17-22]. A major challenge in imaging the localization of mitochondrial mRNAs is the small diameter of mitochondria, which necessitates the use of diffraction-unlimited super-resolution microscopy (nanoscopy) in most instances [23].

In this study, we tailored single molecule FISH (smFISH) of mitochondrial mRNAs for the use with STED and MINFLUX super-resolution microscopy. We report on several applications of smFISH in combination with STED microscopy, including the analysis of mRNA distribution and localization in cells with globally perturbed mitochondrial gene expression, in patient primary cells carrying a single t-RNA mutation as well as in apoptotic cells. Furthermore, we show that the overall shape and the distribution of mitochondrial mRNAs and associated proteins can be analyzed in the single-digit nanometer range using dedicated smFISH probes with MINFLUX nanoscopy.

Results and Discussion

STED microscopy of mitochondrial mRNAs with smFISH

To robustly visualize the submitochondrial distribution of single mitochondrial mRNAs (mRNAs), we adapted branched DNA (bDNA) smFISH labeling for STED microscopy[24-26]. In bDNA FISH, pairs of primary probes hybridize to two adjacent regions of 20 to 30 nucleotides of the target RNA (Fig. 1A). Only pairs of primary probes properly bound to the target RNA are effectively hybridized by a preamplifier, thereby ensuring high specificity. For each mRNA, a different number of probe pairs (3-22) was used, based on the transcript length and sequence

(Table 1), thereby ensuring a high transcript detection probability[24]. To ensure an optimal signal-to-noise ratio, preamplifiers were hybridized with multiple amplifiers, which in turn were hybridized with multiple label probes, each coupled to STED compatible fluorophores, resulting in an assembled amplification "tree" (Fig. 1A).

Using this approach, we imaged three different mitochondrial mRNAs which are transcribed from the mtDNA heavy strand in U-2 OS cells (Fig. 1B). In the three-color STED images, the individual mRNAs could be visualized as clearly discernible structures (Fig. 1C). Most mRNAs were spatially separated from one another; however, instances of close proximity between different pairs or even triplets of mRNAs were also observed (Fig. 1D).

In the STED images, the average diameter (full width at half maximum) of the fluorescence distribution of a single mitochondrial mRNA was about 85 nm, suggesting a high level of mRNA compaction (Fig. 1E). Likewise, the spatially confined mRNA signal demonstrates that the probes do not result in an excessive enlargement of the structure and shows the necessity for employing super-resolution microscopy. Analysis of the minimum distances between the mRNAs revealed that the pairwise distances of all three mRNAs showed similar distributions with a median of around 200 nm (Fig. 1F). The pairwise distances between different mRNA species are similar to the pairwise distances of the same mRNA species (Suppl. Fig. 1A). The similarity in mRNA distances, irrespective of gene proximity on the mtDNA and also between those derived from distinct primary transcripts, are fully in line with previous findings that mitochondrial mRNAs are immediately excised from the primary transcript[10,13,27,28].

To further confirm the specificity of the smFISH probes for imaging mitochondrial mRNAs, we targeted all 13 mitochondrial mRNAs at once in wild-type (WT) U-2 OS control cells and in U-2 OS cells without mtDNA (Rho0 cells) and consequently without mRNAs. In WT cells, this led to a strong signal throughout the mitochondrial network, whereas in Rho0 cells we observed a complete loss of signal, confirming the absence of non-specific probe binding (Suppl. Fig. 1B). To validate the specificity further, we tested a probe for rat *mt-Co3* mRNA on human cells (Suppl. Fig. 1C). Full length human *MT-CO3* and rat *mt-Co3* have a sequence homology of 78 %. Despite the high sequence similarity, we were unable to detect any signal in human cells with the anti-rat smFISH probe, further confirming the high specificity of the probes.

To investigate, if the established labeling and imaging protocols can be combined with the labeling of proteins and are transferable to other cell types, cells were labeled with probes targeting *MT-COX1* or *MT-CYB*, as well as with antibodies labeling dsDNA and proteins such as

GRSF1 and TOM20, respectively (Suppl. Fig. 2). We employed the smFISH probes on several widely used cell types such as HEK-293, HeLa, human primary fibroblasts, as well as on rat hippocampal neurons and combined smFISH with immunolabeling. In all sample types we were able to label the mRNAs together with mitochondrial proteins and/or mtDNA and visualize their specific distributions using STED microscopy (Suppl. Fig. 2).

Together, a robust smFISH protocol for three-color STED super-resolution imaging of three different mitochondrial mRNAs or mRNAs in combination with immunolabeling of mitochondrial DNA and proteins has been established.

MINFLUX imaging of mitochondrial mRNAs

STED-smFISH facilitated the analysis of the distribution of mitochondrial mRNAs within the mitochondrial network. As the achievable resolution of 2D-STED nanoscopy in cellular samples is generally limited to around 30-40 nm[29], this approach is not suited to visualize the fold of a single mRNA.

MINFLUX nanoscopy enables the localization of fluorophores with single-digit precision in 3D by using a local excitation minimum for localization, making it the most photon-efficient super-resolution technique available[30]. The attainable nominal resolution is an order of magnitude higher than in STED microscopy, although at the cost of long recording times. In MINFLUX nanoscopy, stochastic switching is utilized. DNA-PAINT has proven to be particularly useful for this purpose and has been shown to enable the detection of multiple targets through sequential MINFLUX imaging[31]. Hence, we developed MINFLUX-smFISH probes with the preamplifier probe directly fused to a DNA-PAINT docking strand (Fig. 2A). This design of smFISH probes for DNA-PAINT MINFLUX allowed for the stochiometric labeling of the probe pairs and ensured a minimal size of the labels.

Using these probes, we sequentially imaged three mitochondrial mRNAs (*MT-ND1*, *MT-CO1*, *MT-CYB*) in segments of mitochondrial tubules (Fig. 2B). In the MINFLUX-smFISH data representation, the localization of a single fluorophore is rendered as one sphere of 10 nm. A cloud of spheres thereby represents the extent and structure of an mRNA. We observed, fully in line with the STED data, often separated individual mRNAs, but also clusters of two or three mRNAs (Fig. 2C). In the MINFLUX data, the experimentally determined median localization precision of the fluorophores was below 3 nm in all three dimensions in all data sets (Fig. 2D). As the fluorophores are close to the mRNA and distributed along its length, the distribution of the

fluorophores reflects the shape of the mitochondrial mRNA. We found that the mRNAs adopted a variety of structures, from compact to elongated (Fig. 2E).

Since in MINFLUX-smFISH the RNA is lined by the fluorophores, we could use the closest fluorophores belonging to different mRNAs to determine the minimum distance between two different mRNAs. As expected, the average minimum distances of different mRNAs determined on MINFLUX-smFISH (median from 75 nm to 91 nm; Fig. 2F) was lower than in STED-smFISH data (median from 184 nm to 226 nm; Fig. 1F), as in the latter the centers of distinct fluorescence distributions were used as reference points. Still, also in the MINFLUX-smFISH recordings no relevant differences in the pairwise minimum distances between the different mRNAs were detected (Fig. 2F), further suggesting that the vast majority of the labelled mitochondrial mRNAs are physically separated from each other.

Interestingly, when we flattened the 3D MINFLUX data into one virtual plain and convolved it with a STED point-spread-function, the resulting minimum distances (median from 89 nm to 143 nm; Suppl. Fig. 3A) were between those found in the MINFLUX and in the genuine STED data. We attribute this to the larger z-volume recorded by MINFLUX imaging, resulting in more data points, and the different labeling strategies.

Labeling of all 13 mitochondrial mRNAs and subsequent MINFLUX imaging showed that the mRNAs are localized in clusters along the mitochondrial tubules (Suppl. Fig. 3B). This became particularly obvious when comparing their distribution with the distribution of the mitochondrial large ribosomal subunit protein bL12m (MRPL12) labeled with a primary labeled specific antibody (Suppl. Fig. 3C). In contrast to mitochondrial mRNAs, bL12m exhibited a homogeneous distribution throughout the mitochondrion. Occasionally, multiple bL12m foci were observed in proximity to mitochondrial mRNAs, potentially indicating the presence of polysomes (Suppl. Fig. 3D).

STED-smFISH: Perturbed processing of the polycistronic transcripts

To determine whether STED-smFISH enables the visualization of changes in the number and distribution of specific mRNAs in cultured U-2 OS cells, we first downregulated the catalytic subunit of mtRNAse P (Protein Only RNase P Catalytic Subunit; PRORP or MRPP3), which cleaves off the tRNAs that intersperse the protein-coding mRNAs at their 5'-end[32-34] (Suppl. Fig. 4A). Previous studies analyzing the average amounts of mRNAs in cells after downregulation of

PRORP reported an increase of mitochondrial mRNAs[27,35]. Fully in line with this, STED-smFISH showed that upon PRORP knockdown the ratio of mRNA clusters to mtDNA clusters was increased 2.1-fold (*MT-ND1*), 1.4-fold (*MT-CO1*), 1.9-fold (*MT-ATP6*), and 1.3-fold (*MT-CYB*) compared to the WT (Fig. 3A, B).

The guanine-rich RNA sequence binding factor 1 (GRSF1) is a signature protein of mRNA granules[10,11,36,37]. We found that the knockdown of PRORP resulted in an aggregation of GRSF1 into large spots and an accumulation of mRNAs at these sites. As these aggregates were surrounded by numerous mtDNAs, the structures remind of previously described RNA granules[10,11]. Such GRSF1 extended, nucleoid surrounded RNA granules were not apparent in unperturbed U-2 OS cells when imaged with STED microcopy, indicating a complex and dynamic behavior of these structures (Fig. 3A).

STED-smFISH: Perturbed processing of mitochondrial transcription

To investigate if also a perturbed mitochondrial transcription influences the localization of mitochondrial mRNAs and GRSF1, we inhibited the mitochondrial DNA-dependent RNA polymerase (POLRMT) in U-2 OS cells with the specific inhibitor IMT1 (inhibitor of mitochondrial transcription 1) [38]. Treatment with 10 µM IMT1 for 20 hours resulted in lower mRNA and mtDNA levels as well as a homogeneous distribution of GRSF1 in the mitochondrial matrix (Suppl. Fig. 4B). Specifically, the number of *MT-CO1* mRNAs and mitochondrial nucleoids was reduced fivefold and twofold, respectively (Suppl. Fig. 4C), fully in line with previous biochemical studies on cell populations, which showed that inhibition of POLRMT causes a strong decrease in mitochondrial mRNAs and a gradual depletion of mtDNA[38].

STED-smFISH in apoptotic cells

Next, we explored STED-smFISH to visualize mitochondrial mRNAs in apoptotic cells. During apoptosis, mitochondria round up and rupture, as the effector proteins BAX and BAK oligomerize and form apoptotic pores, leading to the release of mitochondrial contents, ultimately resulting in cell death. While the release of nucleoids into the cytoplasm during apoptosis has been shown using super-resolution microscopy[39], little is known about the release of mRNAs, and in particular imaging-based approaches to study this process are lacking. Therefore, we investigated whether STED-smFISH allows to visualize the release of mRNAs during apoptosis.

To induce apoptosis, U-2 OS cells were treated for 16 h with 20 µM Actinomycin D (ActD) and 10 µM ABT-737. After chemical fixation, we labelled for *MT-CO1* mRNA, BAX, and the mitochondrial outer membrane protein TOM22. As expected, mitochondria in apoptotic cells fragmented and BAX accumulated on the mitochondrial outer membrane (Fig. 3C). Using STED-smFISH, we visualized *MT-CO1* mRNAs in the apoptotic cells. The recordings demonstrate that *MT-CO1* mRNAs were indeed partially released during apoptosis and were often found near the BAX pores (Figure 3C). Concomitantly, the number of *MT-CO1* mRNAs confined by the mitochondrial outer membrane decreased by 65 % (Figure 3D).

Taken together, these examples of cultured cells treated with inhibitors of mtDNA replication and mitochondrial transcription, or inducers of apoptosis demonstrate that STED-smFISH is able to reveal changes in the number and localization of mitochondrial mRNAs along with mitochondrial proteins.

STED-smFISH demonstrates changed mRNAs distributions in patient cells

Finally, to investigate the potential of STED-smFISH for the study and characterization of cells of clinical relevance, we analyzed mRNA abundances in primary fibroblasts derived from a patient harboring a single point mutation (m.14709T>C) in the mitochondrially encoded tRNA-Glu (MT-TE) [40,41]. For this, we labeled *MT-CO1* mRNA together with mtDNA and GRSF1 (Fig. 3E). We found a small, but significant decrease in *MT-CO1* mRNAs in the diseased mitochondria compared to mitochondria in healthy control cells (Fig. 3F). This reduction is also reflected in the ratio of the number of mRNA clusters to the number of mtDNA clusters (Suppl. Fig. 4D). Moreover, the number of nucleoids per mitochondrial area is increased in the diseased cells (Suppl. Fig. 4E), while the number of GRSF1 clusters per mitochondrial area is reduced in these cells (Suppl. Fig. 4F). Thus, the STED-smFISH data suggests that a single point mutation in a mitochondrial tRNA leads to defects in mRNA processing and thus to a lower abundance of mRNA and other factors involved in mitochondrial gene expression. STED-smFISH enables the visualization of such subtle differences.

Conclusion

In summary, we developed robust FISH protocols for multi-color imaging of single mitochondrial mRNAs using STED and MINFLUX super-resolution microscopy. The data indicate a tight folding of the mRNAs and reveal the distribution of mRNAs in cells. We can

identify subtle differences in the distribution of mRNAs in challenged cultured mammalian cells as wells as in cells from patients with mitochondrial disorders. The method paves the way to study RNA metabolism and mitochondrial transcription with unprecedented spatial resolution *in cellulo*.

Acknowledgements

We thank the facility for Synthetic Chemistry of the MPI-NAT for coupling of the label probes. We thank Ellen Rothermel, Nicole Molitor and Anne Folmeg for technical support. We are grateful to Stefan W. Hell for continuous support and discussions. This work was supported by the European Research Council (ERCAdG No. 835102) (SJ), (ERCAdG No. 101054637) (PR), by the German Center for Neurodegenerative Diseases, DZNE (JG), by the DFG-funded FOR2848 (P04, PR and SJ), TRR 274 (B02, JG), SFB 1286 (A05, SJ; A06, PR), by the German Center for Child and Adolescent Health, DZKJ (SJ, JG, PR) (BMBF 01GL2402A) and by the DFG under Germany's Excellence Strategy - EXC 2067/1- 390729940 (SJ, JG, PR).

Author contributions

PR and SJ designed research. SJ supervised the study. SS, FM, AC, SVS, and DCJ performed research. SS, FM, MW, PI, and DCJ analyzed data. JG and PR provided materials. SS, FM, SVS, DCJ, and SJ wrote the manuscript. All authors edited and approved the final manuscript.

Declaration of interests

The authors declare no competing interests.

Data availability

All primary data will be available upon reasonable request from the corresponding author.

Code availability

Upon publication of the manuscript, the STED data analysis code and the MINFLUX data processing and analysis code will be available from a public repository.

Figure legends

Figure 1: STED-smFISH.

(A) Schematic representation of the STED-smFISH probe design and probe binding. From left to right: Both strands of the circular mtDNA are transcribed into polycistronic mRNAs, which are further processed to generate 13 mature mRNAs. The STED-smFISH probes consist of probe pairs (blue) that target a specific mRNA (magenta). Several probe pairs, depending on the length of the transcript, can bind simultaneously. Only when both probes of a pair are bound, the preamplifier (black) can bind. Multiple amplifier strands (orange) then bind to the preamplifier. The probe 'tree' is completed by the binding of the label probes (red), which are coupled to the fluorophore of choice (red stars). Specific probe pairs are available for all 13 mRNAs (see Table 1). HSP: heavy strand promoter, LSP: light strand promoter. **(B)** Three-color confocal overview image of a U-2 OS cell labeled for the mRNAs *MT-ND1* (yellow), *MT-CO3* (magenta), and *MT-CYB* (cyan). **(C)** Comparison between the STED and the confocal image at a higher magnification of the indicated area in (B). **(D)** Exemplary close-ups of spatially separated mRNAs (left) and mRNA clusters (right). **(E)** Full width half maximum (FWHM) of *MT-ND1*, *MT-CO3* and *MT-CYB* mRNA spot sizes. **(F)** Quantification of the minimum pairwise distances between *MT-ND1*, *MT-CO3*, and *MT-CYB* mRNAs. Box: 25/75 percentile; whiskers: max/min without outliers; line: median; square: mean (E, F). Curved line: kernel density estimation representing the data point distribution (F). Scale bars: 5 µm (B), 1 µm (C), 50 nm (D).

Figure 2: MINFLUX-smFISH.

(A) Schematic representation of the MINFLUX-smFISH probe design. MINFLUX-smFISH probes consist of probe pairs (blue) targeting a specific mRNA (magenta). Both probes of a pair must bind to the mRNA in order for the preamplifier to bind. The preamplifier for MINFLUX-smFISH is contiguous with a docking strand for DNA-PAINT (orange). The complementary imager strand (red), which is coupled to a single fluorophore (red star), transiently binds to the docking strand. **(B)** 3D rendition of MINFLUX localizations of sequentially acquired *MT-ND1*-, *MT-CO1*-, and *MT-CYB*-mRNAs data in a mitochondrial segment (rendered with sphere diameters of 10 nm). **(C)** Close-ups of several sites from (B). **(D)** Histogram of the distribution of combined localization precisions of MINFLUX data. Dashed lines: median localization precisions. Magenta: axial localization precision (median = 1.1 nm). Cyan: radial localization precision (median = 2.8 nm). **(E)** Example close-ups from (B) showing different shapes of *MT-*

CYB mRNA reflected by the fluorophore positions. **(F)** Quantification of the minimum pairwise distances between *MT-ND1*, *MT-CO3*, and *MT-CYB* mRNAs. Box: 25/75 percentile; whiskers: max/min without outliers; line: median; square: mean; curved line: kernel density estimation representing the data point distribution (F). Sphere diameter = 10 nm (B, C, E).

Figure 3: STED-smFISH to visualize nanoscale changes in mitochondrial mtRNA localizations. **(A)** STED-smFISH of U-2 OS cells: control cells treated with scrambled siRNA and PRORP knockdown (KD) cells, labeled for *MT-ND1* mRNA (yellow), GRSF1 (magenta), and mtDNA (cyan). **(B)** Quantification of the *MT-ND1*, *MT-CO1*, *MT-CYB*, and *MT-ATP6* mRNA cluster to mtDNA cluster (nucleoid) ratio in control cells (Ct) and in PRORP KD cells (KD). **(C**) STED image (overview and magnifications as indicated) of an apoptotic U-2 OS cell (treated with ActD, ABT-737, and Q-VD-OPh for 16 h). Cells were labelled for BAX (magenta), TOM22 (gray), and *MT-CO1* mRNA (yellow) and show *MT-CO1*-mRNA signals outside of the confines of the mitochondrial outer membrane (arrowhead). **(D)** Quantification of *MT-CO1* mRNA clusters per mitochondrial area in untreated control (Ct) cells and apoptotic (Ap) cells. **(E)** STED-smFISH of *MT-CO1* mRNA (yellow) together with immunolabeling for GRSF1 (magenta) and mtDNA (cyan) in cultured human fibroblasts, derived from a control (left) and a patient sample (right) carrying the m.14709T>C mutation in gene MT-TE encoding the tRNA-Glu. **(F)** Quantification of *MT-CO1*-mRNA clusters per mitochondrial area in control fibroblasts (Ct) and fibroblasts from the patient (Pt). Box: 25/75 percentile; whiskers: max/min without outliers; line: median; square: mean; ****: p-value ≤0.0001; ***: p-value ≤0.001 (B, D, F). Scale bars: 1 µm (A, C overview, E) and 500 nm (C close-ups).

Materials and methods

Cell culture

Four different kinds of human cells were used for this study: Human osteosarcoma cells (U-2 OS), human cervical cancer cells (HeLa), human embryonic kidney 293 (HEK-293) cells, human WT fibroblasts, and human WT fibroblasts from a patient with the substitution mutation m.14709T>C (Gen MT-TE in the mitochondrial tRNA coding sequence. HeLa, HEK-293, and human fibroblasts were cultivated at 37 °C and 5 % CO_2 in DMEM, containing 4.5 g/L Glucose and GlutaMAX™ additive (Thermo Fisher #10566016), supplemented with 1 mM sodium pyruvate (Sigma Aldrich #S8636) and 10% (v/v) (FBS) (Bio&SELL #FBS.S0615). U-2 OS cells

were cultivated at 37 °C and 5 % CO_2 in McCoy's medium (Thermo Fisher Scientific #16600082) supplemented with 1 mM sodium pyruvate and 10 % (v/v) FBS.

Hippocampal Neuron Culture

WT *Rattus norvegicus* (strain Wistar) pups were sacrificed at p0 and the hippocampi from both hemispheres were extracted in cooled HBSS buffer (Thermo Fisher Scientific #14175095). The hippocampi were digested in 0.25 % trypsin (Thermo Fisher Scientific #15090046) for 18 min at 37 °C. Afterwards, the digestion was blocked by adding DMEM (Thermo Fisher Scientific #31966047) and after centrifugation and washing with HBSS buffer, the hippocampi were mechanically dissected by pipetting up and down with a serological pipette in Neurobasal medium (Thermo Fisher Scientific #12349015). The cell suspension was plated onto sterile cover slips (1.5H 18 mm cover slips, Marienfeld #0117580) coated with 100 µg/mL Poly-L-ornithine (Merck Millipore #A-004-C). After 1 hour, the medium was changed to Neurobasal medium supplemented with 1× GlutaMAX (Thermo Fisher #35050061), 1× Pen/Strep (Merck Millipore #P0781), 1× B27 supplement (Thermo Fisher #11530536) and cells were grown for 19 days.

KD with siRNAs

U-2 OS cells were seeded on cover slips and let attach overnight. They were then treated with gene specific siRNA pools or negative control siRNA (siTOOLS Biotech, PRORP: Gene ID: 9692, bL12m: 6182). The siRNAs were pre-diluted in ddH_2O and then to a concentration of 48 nM in OptiMEM (ThermoFisher #11058021). The solution was mixed with Lipofectamine RNAiMAX (Invitrogen #13778150) (diluted in OptiMEM, according to the manufacturer's protocol) to a concentration of 24 nM, vortexed for 30 sec, and added to the cells in culture medium to a final concentration of 6 nM. The cells were incubated for 6 days in case of the PRORP KD. For the bL12m KD, cells were transfected again after 3 days and incubated for 8 days in total.

Rho0 cells

U-2 OS POLRMT knockout cells were used as Rho0 cells. The POLRMT KO cell line was created using CIRSPR/Cas9. In short, the Benchling (Benchling, Inc.) tool was used to design guide RNAs (oligos) and their reverse complements for the target gene (POLRMT). The guide RNA and its reverse complement were hybridized in the thermocycler and cloned into the pX458

pSpCas9(BB)-2A-GFP (Addgene, plasmid #48138) plasmid. Cells were transfected with the cloned plasmid, containing the respective guide RNA and Cas9 nuclease. JetPrime (Polyplus-trasfection #101000046) reagent was used for the transfection according to manufacturer´s instructions. Cells expressing Cas9-EGFP were single-cell sorted in 96-well plates using a benchtop Sony SH800S Cell Sorter (Sony Biotechnology Inc.) three days after transfection. After clonal cell expansion, the single-cell clones were confirmed by immunoblotting, PCR of the target gene, sub-cloning with TOPO® (Zero Blunt™ TOPO™ PCR Cloning Kit, Invitrogen™) vector and subsequent Sanger sequencing.

Apoptosis induction

U-2 OS cells were treated for 16 hours with 20 µM ActD (Merck Millipore #A1410), 10 µM ABT-737 (APExBIO #A8193) to induce apoptosis and 10 µM pan-caspase inhibitor (Q-VD-OPh) (APExBIO #A1901) to prevent the detachment of the cells from the coverslip.

Western Blotting

U-2 OS cells were harvested and lysed in lysis buffer (50 mM TRIS [VWR #103156X], 1% sodium dodecyl sulfate (SDS) [Serva #20765], 0.1 mM dithiothreitol [AppliChem #A1101,0025], 4 mM $MgCl_2$ [Thermo Fisher #AM9530G], 1× cOmplete protease inhibitor [Merck #11873580001], 4 mM phenylmethylsulfonyl fluoride [Thermo Fisher #36978], 0.01 U/µL benzonase nuclease [Merck #E1014]) for 2 hours at 4 °C. The protein concentration was determined by utilizing the QubitTM Protein Broad Range (BR) Assay Kit (Thermo Fisher #Q33211). The samples (20 µg) were mixed with 4× Laemmli buffer (0.25 M TRIS [VWR #103156X], 0.28 M SDS [Serva #20765], 40 % glycerol [VWR #24385.295], 20 % 2-mercaptoethanol [Sigma Aldrich #M6250-100Ml], 6 mM bromophenol blue [AppliChem #A3640,0025]) and denatured for 10 min at 95 °C. The samples were loaded on the NuPAGETM 4 to 12 % Bis-TRIS gel (Thermo Fisher #WG1401BX10) and run with 1× NuPAGE™ 2-Morpholinoethanesulfonic acid monohydrate (MES) SDS running buffer (Thermo Fisher #NP0002) at 130 V for 75 min. Afterwards, the gel was washed in 20 % ethanol for 10 min and transferred on nitrocellulose membrane with the iBlotTM transfer stack (Thermo Fisher #IB301001) at 20 V for 1 min, 23 V for 4 min, and 25 V for 2 min. The membrane was washed in ddH20 and 1× TRIS buffered saline (TBS) (Thermo Fisher #J60764.K2), followed by 2 hours blocking in 5 % milk in TBS with Tween (TBST) (Thermo Fisher #J77500.K2) at room

temperature. After 15 min washing in 1× TBST, the membrane was incubated with the primary antibodies diluted in 2 % milk in TBST overnight at 4 °C. After three times washing in TBST for 10 min, the membrane was incubated with secondary antibodies diluted in 2 % milk in TBST for 1 hour at room temperature. Lastly, the membrane was washed again in TBST, incubated for 1 min in Immobilon Forte Western HRP Substrate (Merck #WBLUF0100), and imaged with the Amersham Imager 600 (GE Healthcare). Antibodies and antibody-dilutions used: anti-β-actin (Sigma Aldrich #A5441, 1:2000), anti-MRPP3 (Abcam #ab185942, 1:1000), goat-anti-rabbit HRP (Jackson ImmunoResearch #111-035-144, 1:10000), goat-anti-mouse HRP (Jackson ImmunoResearch #115-035-062, 1:10000).

Design of probe pairs used in this study for smFISH

Probe pairs were designed according to the *View RNA™ Cell Plus Assay* by ThermoFisher (Table 1). The number of simultaneously bound probe pairs per mRNA ranged from 3 to 18 depending to the length and sequence of the transcript. Accordingly, the transcript coverage by the probe pairs ranges from 25 to 70%.

Table 1: Design of probe pairs used in this study for smFISH

Gene name	Length in nt	Number of simultaneously bound probe pairs	Transcript coverage by probe pairs (nt)	Transcript coverage by probe pairs (%)
MT-ND1	954	7	322	34
MT-ND2	1041	9	417	40
MT-ND3	345	5	243	70
MT-ND4L	294	5	201	68
MT-ND4	1377	7	343	25
MT-ND5	1809	5	451	25
MT-ND6	522	3	137	26
MT-CO1	1539	15	696	45
MT-CO2	681	4	188	28
MT-CO3	783	5	221	28
Mt-Co3 (rat)	814	16	683	84
MT-ATP8	204	3	143	70
MT-ATP6	678	5	218	32
MT-CYB	1140	18	767	67
Mt-CyB (rat)	1157	22	954	82

Coupling of dyes to label probes for STED-smFISH

To generate custom label probes with dyes suitable for STED microscopy, 5'-amino functionalized label probe DNA (5' Amino Modifier C6) of Type 1, Type 4, and Type 6 (*ViewRNA Cell Plus Assay*) were purchased from ThermoFisher (custom order). Labeling of the functionalized label probe DNA with a fluorophore was performed as reported earlier for the labeling of 3'-amino functionalized oligonucleotides[42]. In brief, the amino-modified DNA (10 nmol) was dissolved in carbonate buffer (100 mM, pH 9.0) and the solution of the respective succinimidyl ester activated dyes (Table 2) in DMF (10 mM) was added. The reaction mixture was incubated at 37 °C in an incubator shaker for 3 hours in the dark. Subsequently, labeled DNA was purified by denaturing PAGE with subsequent gel extraction and ethanol precipitation.

Table 2: List of fluorophores used for labeling

Fluorophore reagent	**Company + Cat. No.**
Alexa Fluor™ 488 NHS ester (succinimidyl ester)	Thermo Fisher Scientific #A20000
Alexa Fluor™ 594 NHS ester (succinimidyl ester)	Thermo Fisher Scientific #A20004
Abberior STAR RED NHS carbonate	Abberior #STRED-0002-1MG

Labeling of samples with smFISH for STED microscopy

RNA FISH labeling was performed using the ViewRNA ISH Cell Plus Assay by ThermoFisher with custom labeled label probes (https://www.thermofisher.com/de/de/home/life-science/cell-analysis/cellular-imaging/in-situ-hybridization-ish/rna-fish/viewrna-cell-assays.html) according to the supplier's protocol with adaptations. Cells were seeded on 1.5H glass cover slips and pre-fixed with 2 % formaldehyde (Merck Millipore #No. 30525-89-4) in 1× PBS for 10 min at 37 °C. After this pre-fixation step, an additional fixation and permeabilization was carried out using the *ViewRNA Cell Plus Fixation/Permeabilization Solution* for 20 min at 37 °C. The cells were then washed 5 times in 1× PBS with *ViewRNA Cell Plus RNase Inhibitor* and then incubated in *ViewRNA Cell Plus Probe Solution* containing the probe pairs (Table 1) for 2 hours at 40 °C. After incubation with the probe pairs, the cells were washed 5 times with *ViewRNA Cell Plus RNA Wash Buffer Solution* followed by incubation in *ViewRNA Cell Plus PreAmplifier Solution* containing the preamplifier, which binds to the bound probe pair, for 1 hour at 40 °C. After 5 times washing in *ViewRNA Cell Plus RNA Wash Buffer Solution*, the cells were incubated in *ViewRNA Cell Plus Working Amplifier Solution*, which contains the amplifier strands biding to the preamplifier, for 1 hour at 40 °C. Lastly, after 5 times washing in View*RNA Wash Buffer Solution* the cells were incubated for 1 hour at 40 °C with *ViewRNA Cell Plus Working Label Probe Mix Solution* with the added custom labeled label probes at 1.5 pmol/µL, 0.5 pmol/µL, and 1 pmol/µL for probe Type 1, 4, and 6 , respectively. After the final 5 washing steps, the samples were either mounted on glass slides (ThermoFisher #11562203) embedded in Mowiol (2.4 g PVA in 6 g glycerol, 6 mL ddH_2O, 12 mL 200 mM Tris Buffer pH 8.5 plus 2.5 % (w/v) DABCO) or immunofluorescence labeling was performed.

Immunofluorescence labeling

Immunofluorescence labeling was performed after smFISH labeling. The samples were blocked for 5 min with 5 % BSA (AppliChem #A1391) in 1× PBS. The cells were then incubated with primary antibodies diluted in BSA for 1 hour at room temperature (Table 3). After 6 times washing in 1× PBS, cells were incubated with secondary antibodies in BSA for 1 hour at room temperature. Afterwards, cells were washed 6 times in 1× PBS, dipped in ddH_2O and mounted (as described above).

Table 3: List of antibodies used for immunofluorescence labeling

Antibody	**Company + Cat. No., dilution**
Primary ms-anti-BAX	Thermo Fisher #MA5-13994, 1:50
Primary ms-anti-dsDNA	Abcam #ab27156, 1:2000
Primary rb-anti-GRSF1	Sigma-Aldrich #HPA036985, 1:400
Primary rb-anti-Mitofusin 2	Cell Signaling Technologies, #9482, 1:100
Primary rb-anti-TOM20	Abcam #ab186734, 1:200
Primary rb-anti-TOM22	Sigma-Aldrich #HPA003037, 1:400
Primary rb-anti-bL12m	Proteintech #14795-1-AP, 1:400
Primary ms-anti-ATP Synthase Subunit beta	Abcam #ab5432, 1:200
Secondary goat-anti-rabbit Alexa488	Molecular Probes #A11034, 1:200
Secondary goat-anti-mouse Oregon Green	Molecular Probes #O6380, 1:200
Secondary goat-anti-rabbit Alexa594	Invitrogen #A11037, 1:200
Secondary sheep-anti-mouse StarRed	Jackson ImmunoResearch #515005062, custom labeled StarRed NHS carbonate Aberrior #STRED-0002-1MG, 1:200

Custom labeling of primary antibody for DNA-PAINT MINFLUX

For ribosome immunofluorescence labeling for MINFLUX together with MINFLUX-smFISH, the rb-anti-MRPL12 (anti-bL12m) antibody was azide-activated with the GlyCLICK Azide activation kit (GENOVIS #L1-AZ1-025) and coupled to the P3 DNA handle[43].

Design of preamplifiers for MINFLUX-smFISH

For MINFLUX-smFISH, the custom preamplifiers of the Type 1, Type 4, and Type 6 (*ViewRNA Cell Plus Assay*) with the DNA-PAINT docking strands P3, P1, and P2, respectively[43], were purchased from Thermo Fisher Scientific.

Labeling of samples for MINFLUX nanoscopy

MINFLUX-smFISH labeling was carried out in the same way as for STED-smFISH until the addition of the preamplifiers (see above). For MINFLUX-smFISH the custom MINFLUX-

smFISH preamplifiers were used (see above). After 5 times washing in *ViewRNA Cell Plus RNA Wash Buffer Solution*, samples were kept in PBS until DNA-PAINT MINFLUX imaging or immunofluorescence labeling with the custom labeled primary antibody was performed as described above. Finally, the samples were kept in PBS until DNA-PAINT MINFLUX imaging.

Confocal/ STED imaging

Confocal imaging was performed using a TCS SP8 (Leica, Wetzlar, Germany) with a HC PL APO CS2 63x/1.40 Oil objective (Leica) or an Abberior Expert Line Quad-Scanning STED microscope (Abberior Instruments) with a UPlanSApo 100x/1.40 Oil objective (Olympus). For confocal imaging with the TCS SP8 (Suppl. Fig. 3B), Alexa Fluor 488 was excited at 496 nm and STAR RED at 633 nm. For the confocal and STED imaging with the Abberior Expert Line STED microscope (all other image data sets), Alexa Fluor 488 was excited at 485 nm, Alexa Fluor 594 at 561 nm and STAR RED at 640 nm. STED was applied at 595 nm (Alexa Fluor 488) or 775 nm (Alexa Fluor 594, STAR RED), respectively. For all STED image acquisitions, a pixel size of 20 nm was used. Recording parameters were used as described [44]. Except for contrast stretching, no further image processing was carried out for visualization.

DNA-PAINT MINFLUX imaging

Sample mounting and 3D MINFLUX measurements were performed as described previously[31]. In brief, an Abberior MINFLUX microscope (Abberior Instruments) was used for imaging. The Imspector software (16.3.11636-m2205-win64-MINFLUX, Abberior Instruments) and the MINFLUX sequence template “seqDefault3d_w2101” were used for the 3D MINFLUX acquisitions. MINFLUX imaging was performed with a 640 nm excitation laser at a laser power of 71 µW (16%) in the first iteration in the sample, and a pinhole size of 0.57 AU (referenced to the emission maximum of Atto 655 at 680 nm; 0.67 in the Imspector software with a reference wavelength of 574 nm) was used. Before mounting them on stage, the cells labeled with probe pair and preamplifier + docking strand and were incubated for 5 min with fiducials for beam stabilization (150 nm gold beads (BBI Solutions #SKU EM.GC150/4)) and washed five times with PBS. Imager strands P1, P2, and P3 (all conjugated to Atto655) were diluted separately in imaging buffer (Massive Photonics) to a concentration of 5 nM and sequentially applied to the sample on the microscope stage. In between the acquisitions, the sample was washed five times

and the next imaging strand was applied. During imaging, beam monitoring on about five gold beads was activated.

Statistical analysis

All experiments were performed at least in triplicates. For each experiment, part of the mitochondrial network of at least 20 cells (in total for each case ≥ 60 cells) was imaged. Statistical analyses were performed using GraphPad Prism 9. The data was checked for normality by visual inspection of Q-Q-Plots. For normally distributed data sets, an unpaired two-tailed t-test was employed. The significance level ****, ***, **, and * correspond to a p-value of ≤0.0001, ≤0.001, ≤0.01, and ≤0.05, respectively. In the cases where kernel density estimation of the data points was performed, this was conducted using a bandwidth selected based on Scott's rule.

STED data analysis

The STED data analysis was performed using as custom written MATLAB script. In short, the STED images were smoothed with a 25 nm FWHM Gaussian filter, and background removal was performed by subtracting a 210 nm FWHM Gaussian filtered image from the smoothed image. mRNA localizations were defined at positions of local maxima in areas that were at least 100 nm away from the image edges and exceeded at least 3 detected counts after background subtraction (Suppl Fig. 5). To determine the mitochondrial area from the (background subtracted) images, a circular area with a radius of 6 pixels (120 nm) around the local maxima was used. Areas smaller than 200 pixels were discarded. The resulting binary mask was convolved with a 5x5 pixel square. The resulting images were thresholded (pixel-intensity 12.5) and thus binarized again. Then, holes in the mitochondrial mask smaller than 200 pixels were filled. The detected mRNA, protein or mtDNA cluster positions inside the mitochondria were counted and divided by the mitochondrial mask area to obtain cluster densities. For distance calculations, the minimum pairwise distances of the detected mRNAs were calculated. The boxplots were created with OriginPro 2020 (64-bit) (OriginLab).

MINFLUX data analysis

The MINFLUX data processing and analysis was performed using as custom written Python script. For each ROI the sequentially acquired MINFLUX data of each channel was aligned based on the gold bead positions from the beam monitoring. Localization precisions were calculated as

previously described[31]. In brief, the individual localizations from each binding event with more than four localizations were combined. The stated localization precision in x, y (s_r) and z (s_z) refers to the median of the localization precisions of the combined localizations. Next, we determined the axis with the worst precision for each dataset and discarded all combined localizations with a precision below two times its mean. To filter out background localizations, the combined localizations of all datasets of one ROI were concatenated and DBSCAN with epsilon of 120 nm and minimum 8 points was performed on the data. The clustered datapoints were used for visualization and further analysis. The minimal Euclidean distance of each (filtered) combined localization to a combined localization of a different dataset of the same ROI was calculated. The minimum distance boxplots were created with OriginPro 2020 (64-bit) (OriginLab) and the combined localizations were plotted using Blender 3.4.1 with a sphere size (diameter) corresponding to 10 nm.

References

1 Anderson, S. *et al*. Sequence and organization of the human mitochondrial genome. *Nature* **290**, 457-465 (1981). https://doi.org:10.1038/290457a0

2 Bogenhagen, D. & Clayton, D. A. The number of mitochondrial deoxyribonucleic acid genomes in mouse L and human HeLa cells. Quantitative isolation of mitochondrial deoxyribonucleic acid. *J Biol Chem* **249**, 7991-7995 (1974).

3 Kaufman, B. A. *et al.* The Mitochondrial Transcription Factor TFAM Coordinates the Assembly of Multiple DNA Molecules into Nucleoid-like Structures. *Molecular Biology of the Cell* **18**, 3225-3236 (2007). https://doi.org:10.1091/mbc.e07-05-0404

4 Kukat, C. *et al.* Super-resolution microscopy reveals that mammalian mitochondrial nucleoids have a uniform size and frequently contain a single copy of mtDNA. *Proceedings of the National Academy of Sciences* **108**, 13534-13539 (2011). https://doi.org:10.1073/pnas.1109263108

5 Falkenberg, M., Larsson, N.-G. & Gustafsson, C. M. Replication and Transcription of Human Mitochondrial DNA. *Annual Review of Biochemistry* **93**, 47-77 (2024). https://doi.org:https://doi.org/10.1146/annurev-biochem-052621-092014

6 Hällberg, B. M. & Larsson, N.-G. Making Proteins in the Powerhouse. *Cell Metabolism* **20**, 226-240 (2014). https://doi.org:https://doi.org/10.1016/j.cmet.2014.07.001

7 Falkenberg, M. *et al*. Mitochondrial transcription factors B1 and B2 activate transcription of human mtDNA. *Nat Genet* **31**, 289-294 (2002). https://doi.org:10.1038/ng909

8 Gustafsson, C. M., Falkenberg, M. & Larsson, N.-G. Maintenance and Expression of Mammalian Mitochondrial DNA. *Annual Review of Biochemistry* **85**, 133-160 (2016). https://doi.org:10.1146/annurev-biochem-060815-014402

9 Rackham, O. & Filipovska, A. Organization and expression of the mammalian mitochondrial genome. *Nature Reviews Genetics* **23**, 606-623 (2022). https://doi.org:10.1038/s41576-022-00480-x

10 Antonicka, H., Sasarman, F., Nishimura, T., Paupe, V. & Shoubridge, E. A. The Mitochondrial RNA-Binding Protein GRSF1 Localizes to RNA Granules and Is Required for Posttranscriptional Mitochondrial Gene Expression. *Cell Metabolism* **17**, 386-398 (2013). https://doi.org:10.1016/j.cmet.2013.02.006

11 Jourdain, A. A. *et al.* GRSF1 Regulates RNA Processing in Mitochondrial RNA Granules. *Cell Metabolism* **17**, 399-410 (2013). https://doi.org:10.1016/j.cmet.2013.02.005

12 Lee, K. W., Okot-Kotber, C., LaComb, J. F. & Bogenhagen, D. F. Mitochondrial ribosomal RNA (rRNA) methyltransferase family members are positioned to modify nascent rRNA in foci near the mitochondrial DNA nucleoid. *J Biol Chem* **288**, 31386-31399 (2013). https://doi.org:10.1074/jbc.M113.515692

13 Jiang, S. *et al.* TEFM regulates both transcription elongation and RNA processing in mitochondria. *EMBO reports* **20**, e48101 (2019). https://doi.org:https://doi.org/10.15252/embr.201948101

14 Stoldt, S. *et al.* Spatial orchestration of mitochondrial translation and OXPHOS complex assembly. *Nature Cell Biology* **20**, 528-534 (2018). https://doi.org:10.1038/s41556-018-0090-7

15 Englmeier, R., Pfeffer, S. & Förster, F. Structure of the Human Mitochondrial Ribosome Studied In Situ by Cryoelectron Tomography. *Structure* **25**, 1574-1581.e1572 (2017). https://doi.org:https://doi.org/10.1016/j.str.2017.07.011

16 Soto, I. *et al.* Balanced mitochondrial and cytosolic translatomes underlie the biogenesis of human respiratory complexes. *Genome Biology* **23**, 170 (2022). https://doi.org:10.1186/s13059-022-02732-9

17 Albus, C. A., Berlinguer-Palmini, R., Chrzanowska-Lightowlers, Z. M. & Lightowlers, R. N. Four-Color STED Super-Resolution RNA Fluorescent In Situ Hybridization and Immunocytochemistry to Visualize Mitochondrial mRNAs in Context with Mitochondrial Ribosomes. *Methods Mol Biol* **2661**, 303-316 (2023). https://doi.org:10.1007/978-1-0716-3171-3_17

18 Kim, Y. *et al.* PKR Senses Nuclear and Mitochondrial Signals by Interacting with Endogenous Double-Stranded RNAs. *Molecular Cell* **71**, 1051-1063.e1056 (2018). https://doi.org:https://doi.org/10.1016/j.molcel.2018.07.029

19 Smirnova, A., Richert, L., Smirnov, A., Mély, Y. & Tarassov, I. in *Mitochondrial Medicine: Volume 3: Manipulating Mitochondria and Disease- Specific Approaches* (eds Volkmar Weissig & Marvin Edeas) 157-173 (Springer US, 2021).

20 Young, A. P., Jackson, D. J. & Wyeth, R. C. A technical review and guide to RNA fluorescence in situ hybridization. *PeerJ* **8**, e8806 (2020). https://doi.org:10.7717/peerj.8806

21 Zhu, X. *et al.* Non-coding 7S RNA inhibits transcription via mitochondrial RNA polymerase dimerization. *Cell* **185**, 2309-2323.e2324 (2022). https://doi.org:https://doi.org/10.1016/j.cell.2022.05.006

22 Zorkau, M. *et al.* in *Mitochondrial Gene Expression: Methods and Protocols* (eds Michal Minczuk & Joanna Rorbach) 159-181 (Springer US, 2021).

23 Jakobs, S., Stephan, T., Ilgen, P. & Bruser, C. Light Microscopy of Mitochondria at the Nanoscale. *Annual Review of Biophysics, Vol 49, 2020* **49**, 289-308 (2020). https://doi.org:10.1146/annurev-biophys-121219-081550

24 Battich, N., Stoeger, T. & Pelkmans, L. Image-based transcriptomics in thousands of single human cells at single-molecule resolution. *Nature Methods* **10**, 1127-1133 (2013). https://doi.org:10.1038/nmeth.2657

25 Player, A. N., Shen, L.-P., Kenny, D., Antao, V. P. & Kolberg, J. A. Single-copy Gene Detection Using Branched DNA (bDNA) In Situ Hybridization. *Journal of Histochemistry & Cytochemistry* **49**, 603-611 (2001). https://doi.org:10.1177/002215540104900507

26 Wang, F. *et al.* RNAscope: A Novel in Situ RNA Analysis Platform for Formalin-Fixed, Paraffin-Embedded Tissues. *The Journal of Molecular Diagnostics* **14**, 22-29 (2012). https://doi.org:https://doi.org/10.1016/j.jmoldx.2011.08.002

27 Sanchez, M. I. G. L. *et al.* RNA processing in human mitochondria. *Cell Cycle* **10**, 2904-2916 (2011). https://doi.org:10.4161/cc.10.17.17060

28 Ojala, D., Montoya, J. & Attardi, G. tRNA punctuation model of RNA processing in human mitochondria. *Nature* **290**, 470-474 (1981). https://doi.org:10.1038/290470a0

29 Sahl, S. J., Hell, S. W. & Jakobs, S. Fluorescence nanoscopy in cell biology. *Nat Rev Mol Cell Biol* **18**, 685-701 (2017). https://doi.org:10.1038/nrm.2017.71

30 Balzarotti, F. *et al.* Nanometer resolution imaging and tracking of fluorescent molecules with minimal photon fluxes. *Science* **355**, 606-612 (2017). https://doi.org:10.1126/science.aak9913

31 Ostersehlt, L. M. *et al*. DNA-PAINT MINFLUX nanoscopy. *Nat Methods* **19**, 1072-1075 (2022). https://doi.org:10.1038/s41592-022-01577-1

32 Holzmann, J. *et al.* RNase P without RNA: Identification and Functional Reconstitution of the Human Mitochondrial tRNA Processing Enzyme. *Cell* **135**, 462-474 (2008). https://doi.org:10.1016/j.cell.2008.09.013

33 Reinhard, L., Sridhara, S. & Hallberg, B. M. Structure of the nuclease subunit of human mitochondrial RNase P. *Nucleic Acids Research* **43**, 5664-5672 (2015). https://doi.org:10.1093/nar/gkv481

34 Chujo, T. *et al.* LRPPRC/SLIRP suppresses PNPase-mediated mRNA decay and promotes polyadenylation in human mitochondria. *Nucleic Acids Research* **40**, 8033-8047 (2012). https://doi.org:10.1093/nar/gks506

35 Rackham, O. *et al.* Hierarchical RNA Processing Is Required for Mitochondrial Ribosome Assembly. *Cell Reports* **16**, 1874-1890 (2016). https://doi.org:https://doi.org/10.1016/j.celrep.2016.07.031

36 Qian, Z. & Wilusz, J. GRSF-1: a poly(A)+ mRNA binding protein which interacts with a conserved G-rich element. *Nucleic Acids Res* **22**, 2334-2343 (1994). https://doi.org:10.1093/nar/22.12.2334

37 Pietras, Z. *et al.* Dedicated surveillance mechanism controls G-quadruplex forming non-coding RNAs in human mitochondria. *Nat Commun* **9**, 2558 (2018). https://doi.org:10.1038/s41467-018-05007-9

38 Bonekamp, N. A. *et al.* Small-molecule inhibitors of human mitochondrial DNA transcription. *Nature* **588**, 712-716 (2020). https://doi.org:10.1038/s41586-020-03048-z

39 McArthur, K. *et al*. BAK/BAX macropores facilitate mitochondrial herniation and mtDNA efflux during apoptosis. *Science* **359** (2018). https://doi.org:10.1126/science.aao6047

40 Hanna, M. G. *et al*. Congenital encephalomyopathy and adult-onset myopathy and diabetes mellitus: different phenotypic associations of a new heteroplasmic mtDNA tRNA glutamic acid mutation. *Am J Hum Genet* **56**, 1026-1033 (1995).

41 Hao, H., Bonilla, E., Manfredi, G., DiMauro, S. & Moraes, C. T. Segregation patterns of a novel mutation in the mitochondrial tRNA glutamic acid gene associated with myopathy and diabetes mellitus. *Am J Hum Genet* **56**, 1017-1025 (1995).

42 Liaqat, A., Stiller, C., Michel, M., Sednev, M. V. & Hobartner, C. N-6-Isopentenyladenosine in RNA Determines the Cleavage Site of Endonuclease Deoxyribozymes. *Angewandte Chemie-International Edition* **59**, 18627-18631 (2020). https://doi.org:10.1002/anie.202006218

43 Jungmann, R. *et al.* Multiplexed 3D cellular super-resolution imaging with DNA-PAINT and Exchange-PAINT. *Nat Methods* **11**, 313-318 (2014). https://doi.org:10.1038/nmeth.2835

44 Schweighofer, S. V., Inamdar, K., Jans, D. C. & Jakobs, S. STED super-resolution microscopy of mitochondrial translocases. *Methods in enzymology* **707**, 299-327 (2024).

Figure 1

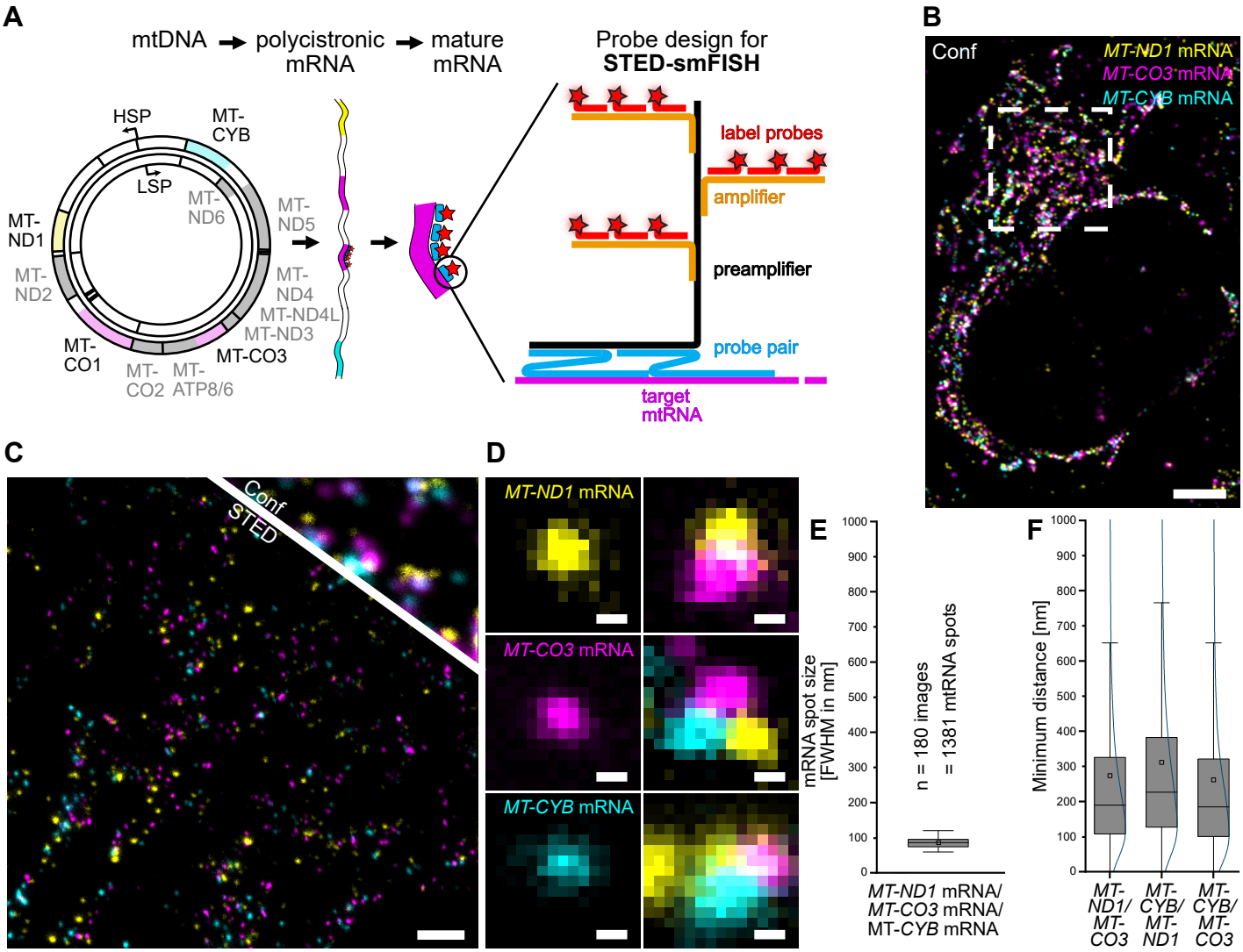
A
mtDNA
polycistronic mRNA
mature mRNA
Probe design for STED-smFISH
HSP
MT-CYB
LSP
MT-ND6
MT-ND5
MT-ND1
MT-ND2
MT-ND4
MT-ND4L
MT-ND3
MT-CO1
MT-CO3
MT-CO2
MT-ATP8/6
label probes
amplifier
preamplifier
probe pair
target mtRNA
B
Conf
MT-ND1 mRNA
MT-CO3 mRNA
MT-CYB mRNA
C
Conf
STED
D
MT-ND1 mRNA
MT-CO3 mRNA
MT-CYB mRNA
E
mRNA spot size [FWHM in nm]
n = 180 images
= 1381 mtRNA spots
MT-ND1 mRNA/ MT-CO3 mRNA/ MT-CYB mRNA
F
Minimum distance [nm]
MT-ND1/ MT-CO3
MT-CYB/ MT-ND1
MT-CYB/ MT-CO3

Figure 2

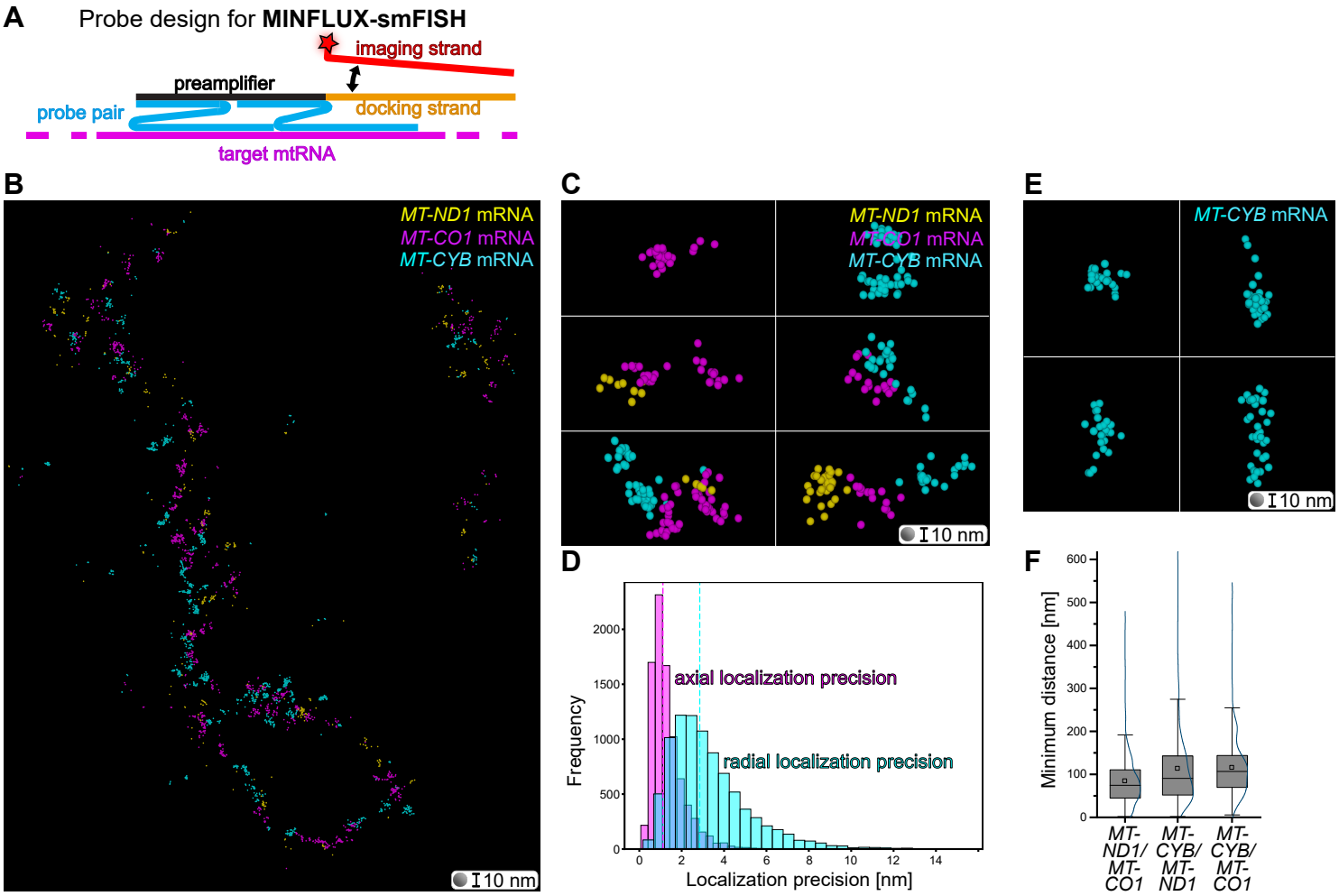
A
Probe design for MINFLUX-smFISH
imaging strand
preamplifier
probe pair
docking strand
target mtRNA
B
MT-ND1 mRNA
MT-CO1 mRNA
MT-CYB mRNA
10 nm
C
MT-ND1 mRNA
MT-CO1 mRNA
MT-CYB mRNA
10 nm
D
axial localization precision
radial localization precision
Frequency
Localization precision [nm]
E
MT-CYB mRNA
10 nm
F
Minimum distance [nm]
MT-ND1/ MT-CO1
MT-CYB/ MT-ND1
MT-CYB/ MT-CO1

Figure 3

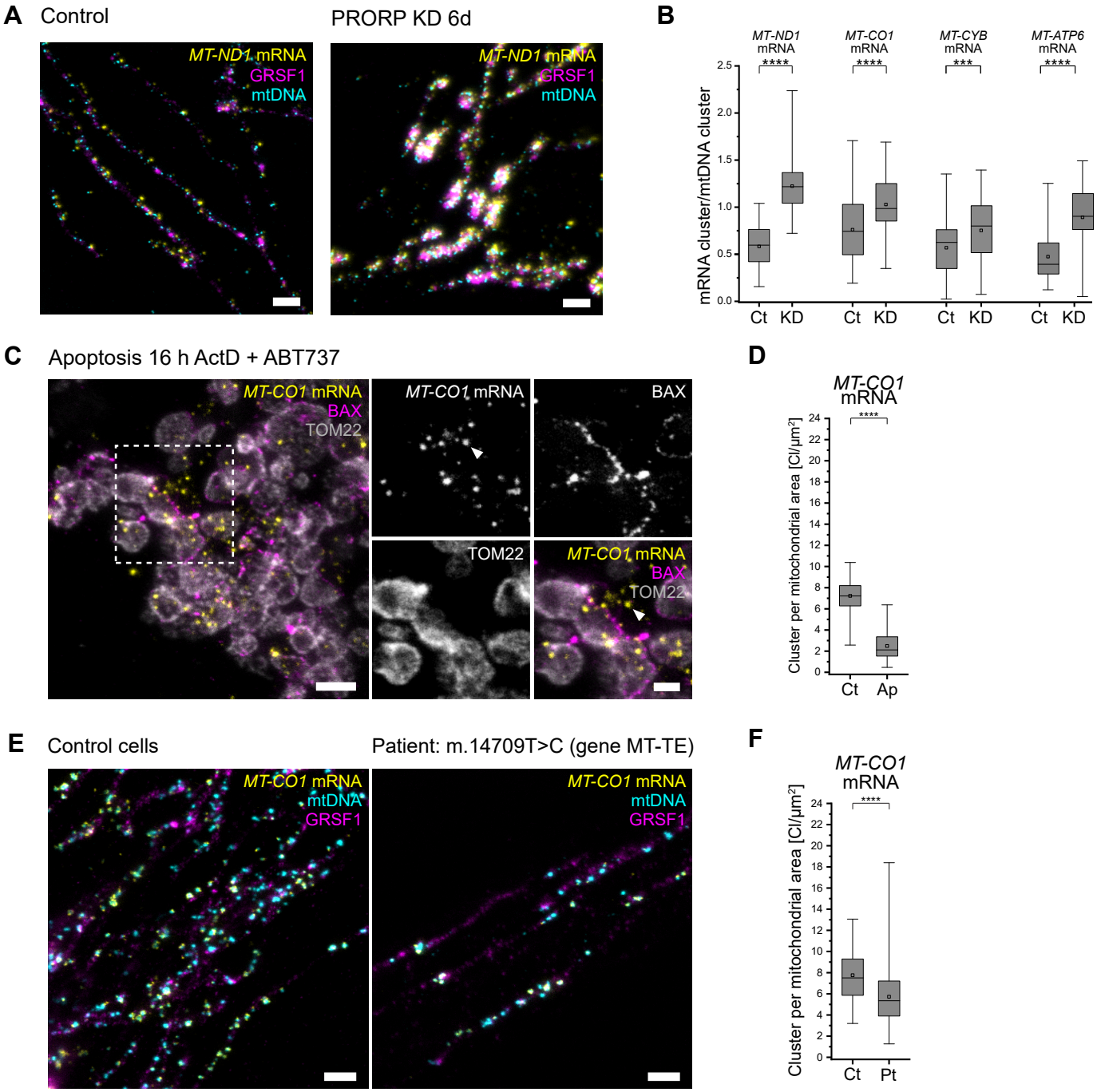
A
Control
PRORP KD 6d
MT-ND1 mRNA
GRSF1
mtDNA
B
MT-ND1 mRNA
MT-CO1 mRNA
MT-CYB mRNA
MT-ATP6 mRNA
mRNA cluster/mtDNA cluster
Ct
KD
C
Apoptosis 16 h ActD + ABT737
MT-CO1 mRNA
BAX
TOM22
D
Cluster per mitochondrial area [Cl/µm²]
Ct
Ap
E
Control cells
Patient: m.14709T>C (gene MT-TE)
F
Pt